RSC Advances

Asymmetric surface effect on the configuration of bilayer Si/SiGe nanosprings

Journal:	*RSC Advances*
Manuscript ID	RA-ART-09-2015-018791.R1
Article Type:	Paper
Date Submitted by the Author:	08-Oct-2015
Complete List of Authors:	Kim, Seongseop; Seoul National University, School of Mechanical and Aerospace Engineering Kim, Wonbae; Seoul National University, School of Mechanical and Aerospace Engineering Chung, Hayoung; Seoul National University, School of Mechanical and Aerospace Engineering Cho, Maenghyo; Seoul National University, School of Mechanical and Aerospace Engineering
Subject area & keyword:	Nanomaterials - Materials < Materials

Asymmetric surface effect on the configuration of bilayer Si/SiGe nanosprings

Seongseop Kim,[a] Wonbae Kim,[a] Hayoung Chung,[a] and Maenghyo Cho[a*]

This study investigates the asymmetric surface effect on nanosprings composed of Si/SiGe bilayer thin films. The misfit strain between Si and SiGe layers is known to be the driving force whereby the deformation into nanospring shape occurs. The crystalline orientation and width-to-thickness ratio are main factors that determine the deformed equilibrium configuration. In addition, as the thickness decreases to dozens of nanometers or less, the effect of the surface on the equilibrium configuration of the thin film is magnified. The diamond cubic crystal structure, unlike the face-centered or body-centered cubic structures, has asymmetric surface properties. Owing to the asymmetry, Si/SiGe bilayers with odd numbers of atomic layers have different surface configurations than those having even numbers of atomic layers. Finite element analysis with the surface effect have been performed to investigate the surface effect on the equilibrium configuration. It is observed that both size and surface configuration affects the equilibrium configuration of bilayer Si/SiGe nanosprings. An unexpected spring shape was observed when the film aligned in the <100> direction, which is unlikely if the surface effect is neglected.

[a] *Division of WCU Multiscale Mechanical Design, School of Mechanical and Aerospace Engineering, Seoul National University, Seoul 151-744, Republic of Korea*

*Corresponding author, e-mail address: *mhcho@snu.ac.kr*

1. Introduction

Nanosprings are a type of nanostructure with a helical shape, which attract interest from various fields owing to their mechanical and chemical characteristics. Chemical sensors[1], temperature sensors[2], artificial bacterial flagella[3], and carrier for biological molecules[4] have been fabricated by using nanosprings.

Various materials and fabrication schemes have been utilized for the fabrication of nanosprings[5-10]. Some researchers[11-15] obtained nanosprings by performing lithography and selective etching on epitaxial bilayer thin films such as Si/SiGe or InGaAs/GaAs. In contrast to other fabrication methods, this method enables control of the shape and position of the nanospring by means of lithography. The elongated rectangular strip is used as the initial pattern. The misfit strain induced by the difference in the lattice constant between layers offers the driving force of rolling deformation of the pattern.[11] The rolling direction is determined by various factors such as material orientation and geometry of the thin film. The pattern tends to roll in the <100> direction, which is the weakest direction in the materials.

Some computer simulation studies have predicted the spring constant of nanosprings.[12, 13, 15, 16] In these studies, experimentally obtained spring geometry was used to prepare the initial model for the simulation. However, these studies cannot predict the equilibrium configuration or residual stress of nanosprings. Kim *et al.*[17] and Chen[18] performed finite element analyses to determine the equilibrium configuration of nanosprings. Kim *et al.* showed that various configurations, such as nanosprings, nanobands, nanorings, and nanopipes, could be obtained from the Si/SiGe bilayer thin film according to the design parameters. They successfully reproduced various configurations, which were obtained experimentally by assuming that the misfit strain was the driving force. Chen fabricated various helical nanoribbons, in which both left and right-handed segments were produced.

However, when the bilayer thickness reaches nanoscale, the surface effect is very important in the equilibrium configuration of nanosprings composed of bilayer thin films. Therefore, the surface effect and the misfit strain should be considered as the driving forces whereby the equilibrium configuration is achieved in the nanoscale regime. Molecular dynamics (MD) and density functional theory (DFT) simulations are commonly used for the study of nanomaterials. However, these atomic simulation methods are not suitable for the study of nanosprings, as the micron or submicron scale of nanosprings requires too much computation time.

Therefore, in this paper we investigated the equilibrium configuration of Si/SiGe bilayer thin films considering the surface effect and the number of atomic layers. The surface effect was determined from atomistic calculations. A finite element analysis (FEA) was performed to obtain the equilibrium configuration, and an MD simulation was performed to verify the FEA in small scale system.

2. Results and discussion

a. Asymmetric surface properties

As the surface effect is expected to be an important factor affecting the equilibrium configuration of Si/SiGe nanosprings, the surface structure and surface properties of Si and SiGe are discussed in this section. As the Si/SiGe bilayer thin film is epitaxially deposited,[11-14] both Si and SiGe layers have a diamond cubic crystalline structure (Fig. 1 (a)). The SiGe is a solid solution of Si and Ge where either Si or Ge randomly occupies the atomic sites of the diamond cubic structure. The lattice constants of Si and Ge are 0.543 and 0.565 nm, respectively.

Though the diamond cubic crystal structure surfaces can have various configurations because of the surface treatment,[19-21] only the unreconstructed *p*(1×1) ideal {100} surface is considered in this study. In the unreconstructed *p*(1×1) ideal {100} surface, the outermost surface atoms are aligned and covalently bonded to the atoms of the second atomic layer, as shown in Fig. 1 (a). Henceforth the direction of the aligned atoms of the outermost atomic layer will be called the α-direction, and the direction perpendicular to this will be called the β-direction, as shown in Fig. 1 (b). The α-direction changes alternately between [110] and $[1\bar{1}0]$ as the number of atomic layers changes. Therefore, the number of atomic layers in the thin film plays a critical role in the equilibrium configuration, and whether even or odd numbers of atomic layers are used must be considered. When a film has an even number of atomic layers, the α-direction in the top and bottom surfaces are parallel to each other, but when an odd number is used, the directions are orthogonal to each other.

We adopted the concept of the core-shell model[22] to express the surface effect, as illustrated in Fig. 2. In the model, the film is divided into surface and bulk layers, which will be referred to as shell and core, respectively. The core-shell model assumes that the shell has a finite thickness. The shell thickness is determined manually by observing the stress profile of a thin film, which is determined by atomistic calculations.[23] It is observed that the effect of the surface reaches virtually no more than the fourth atomic layer from the surface. Therefore, the outermost four atomic layers are considered the surface section, and thus the thicknesses of Si and Ge surfaces are 0.543 and 0.565 nm, respectively. The thickness of SiGe is determined by the rule of mixture from the thicknesses of Si and Ge.

The surface and bulk material properties are determined by atomistic calculations. Tersoff potential[24] is used as the interatomic potentials of Si and Ge. The calculated stiffness tensor values of the five outermost atomic layers of Si and Ge are given in Tables 1 and 2, respectively. In the core-shell model, it is assumed that the shell has averaged material properties throughout its thickness. The averaged surface stiffness tensors and surface stresses are defined as follows:

$$\underset{\sim}{C}_{shell} = \frac{1}{n}\sum_{i=1}^{n} \underset{\sim}{C}^{(i)} \quad (1)$$

$$\underset{\sim}{\tau}^{\circ}_{shell} = \frac{1}{n}\sum_{i=1}^{n} \tau^{(i)} \quad (2)$$

where C_{shell} and τ°_{shell} are the stiffness tensor and stresses of the shell, respectively, $C^{(i)}$ and $\tau^{(i)}$ are the stiffness tensor and stresses of the i^{th} atomic layer, respectively, and n is the number of atomic layers of the surface. The calculated material properties of Si, Ge, and SiGe are shown in Tables 3–5. The material properties of SiGe are calculated from those of Si and Ge by applying the rule of mixture. The tables show the properties measured both in the {100}/<100> and {100}/<110> directions, and the three coordinate axes, 1, 2, and 3, in {100}/<110> correspond to α, β, and z, respectively. Tables 3 and 4 show the bulk and surface material properties, respectively. The fact that the shear stresses in the <110> direction are zero (Table 5) implies that <110> are the principal directions of the surface stresses for each material. In addition, α is the stiffest direction in the {100} surface for each material.

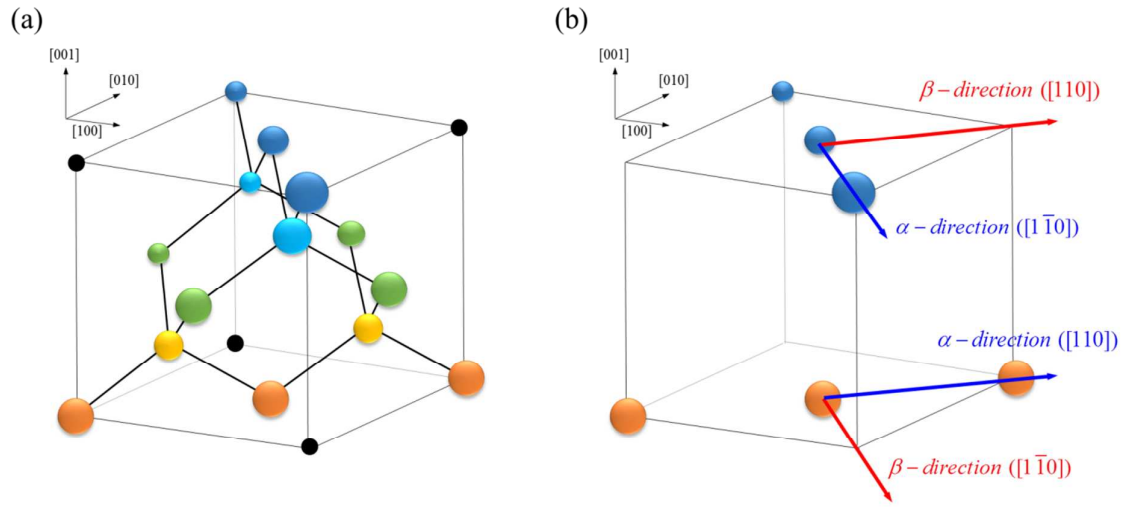

Figure 1. (a) Illustration of the diamond structure showing the atoms aligned in each atomic layer. The direction changes alternately between [110] and [$1\bar{1}0$] for each atomic layer. (b) The direction of the atom alignment and the direction perpendicular to the atom alignment are denoted as α-direction and β-direction, respectively. This illustration shows that both α and β directions are in <110>, and the direction of α and β are exchanged when a film contains an odd number of atomic layers.

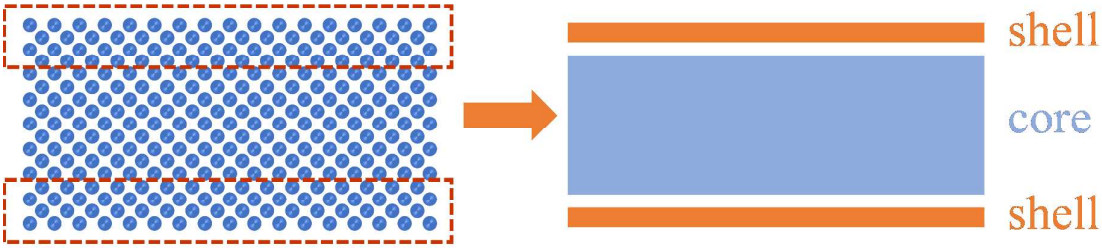

Figure 2. Explanation of the core-shell model. Surface and bulk parts in the atomic model (left) are simplified as shell and core (right), respectively, in the core-shell model. The shell has a finite thickness, and averaged surface properties are assigned to this region.

Table 1. Stiffness tensor values of the five outermost atomic layers of Si measured in GPa. Properties are measured in {100}/<110>.

	$C_{11}^{(i)}$	$C_{22}^{(i)}$	$C_{33}^{(i)}$	$C_{12}^{(i)}$	$C_{13}^{(i)}$	$C_{23}^{(i)}$	$C_{44}^{(i)}$	$C_{55}^{(i)}$	$C_{66}^{(i)}$
1st	149.0	0.0	-14.0	0.0	-8.5	0.0	-5.0	-5.0	0.0
2nd	209.3	179.7	147.4	45.7	90.5	78.6	62.3	73.9	36.6
3rd	178.5	175.6	142.1	39.6	75.3	74.4	68.4	69.6	33.4
4th	178.9	178.3	142.8	40.1	75.8	75.6	68.9	69.1	33.7
5th	178.0	178.2	142.6	40.0	75.4	75.5	69.1	69.0	33.6

Table 2. Stiffness tensor values of the five outermost atomic layers of Ge measured in GPa. Properties are measured in {100}/<110>.

	$C_{11}^{(i)}$	$C_{22}^{(i)}$	$C_{33}^{(i)}$	$C_{12}^{(i)}$	$C_{13}^{(i)}$	$C_{23}^{(i)}$	$C_{44}^{(i)}$	$C_{55}^{(i)}$	$C_{66}^{(i)}$
1st	171.7	0.0	-1.1	0.0	-0.4	0.0	-0.4	-0.4	0.0
2nd	182.1	156.7	142.6	25.1	57.4	50.5	61.8	71.5	50.6
3rd	159.0	156.0	137.9	24.6	43.9	43.9	66.2	67.2	46.8
4th	159.0	158.4	138.8	24.6	44.7	44.6	66.8	66.9	47.2
5th	158.2	158.4	138.5	24.6	44.4	44.4	66.8	66.8	47.1

Table 3. The bulk (or core) stiffness tensor values of Si, Ge, and SiGe measured in GPa. Properties are measured both in {100}/<100> and {100}/<110>. The composition ratio of SiGe is Si:Ge = 1:1.

	C_{11}^{core}	C_{33}^{core}	C_{12}^{core}	C_{13}^{core}	C_{44}^{core}	C_{66}^{core}
$Si^{<100>}$	142.5	-	75.4	-	69.0	-
$Ge^{<100>}$	138.5	-	44.4	-	66.8	-
$SiGe^{<100>}$	140.5	-	59.9	-	67.9	-
$Si^{<110>}$	178.0	142.5	39.9	75.4	69.0	33.6
$Ge^{<110>}$	158.2	138.5	24.6	44.4	66.8	47.0
$SiGe^{<110>}$	168.1	140.5	32.3	59.9	67.9	40.3

Table 4. The shell stiffness tensor values of Si, Ge, and SiGe measured in GPa. Properties are measured both in {100}/<100> and {100}/<110>. The composition ratio of SiGe is Si:Ge = 1:1.

	C_{11}^{shell}	C_{22}^{shell}	C_{33}^{shell}	C_{12}^{shell}	C_{13}^{shell}	C_{23}^{shell}	C_{44}^{shell}	C_{55}^{shell}	C_{66}^{shell}
$Si^{<100>}$	119.7	-	104.6	67.8	57.7	-	50.3	-	62.4
$Ge^{<100>}$	116.9	-	104.6	44.6	35.6	-	50.0	-	62.1
$SiGe^{<100>}$	118.3	-	104.6	56.2	46.6	-	50.1	-	62.3
$Si^{<110>}$	178.9	133.4	104.6	31.4	58.3	57.2	48.7	51.9	25.9
$Ge^{<110>}$	167.9	117.8	104.6	18.6	36.4	34.8	48.6	51.3	36.1
$SiGe^{<110>}$	173.4	125.6	104.6	25.0	47.3	46.0	48.6	51.6	31.0

Table 5. Shell stress of Si, Ge, and SiGe measured in GPa. Properties are measured both in {100}/<100> and {100}/<110>. The composition ratio of SiGe is Si:Ge = 1:1.

	$\overset{\circ}{\tau}_{11}$	$\overset{\circ}{\tau}_{22}$	$\overset{\circ}{\tau}_{12}$
$Si^{<100>}$	-1.66	-1.66	1.84
$Ge^{<100>}$	-0.62	-0.62	0.68
$SiGe^{<100>}$	-1.14	-1.14	1.26
$Si^{<110>}$	-3.50	0.18	0.00
$Ge^{<110>}$	-1.30	0.06	0.00
$SiGe^{<110>}$	-2.40	0.12	0.00

b. Modeling of the finite element method with the surface effect

The modeling details for the misfit strain are explained in the paper by Kim *et al.*[17] Regarding the surface effect, the composite shell element, which can handle multiple layers, is used to apply the core-shell model. The surface and bulk material properties presented in Tables 3–5 are applied to the shell and core, respectively. ABAQUS software[25] was used to perform FEA with the surface effect (FEAwSE).

A few surface configurations are chosen as follows to demonstrate the effect of asymmetric surface properties. In the case that a Si/SiGe strip is aligned in the <100> direction, two different surface configurations are possible: even layers and odd layers. They will be called <100>/αα and <100>/αβ, respectively, throughout the paper. Illustrations of the surface configurations are given in Fig. 3.

On the other hand, when the strip is aligned in the <110> direction, the α-direction of each surface stress can be either widthwise or lengthwise. Therefore, four different surface configurations are possible: even layers with lengthwise α-direction, even layers with widthwise α-direction, odd layers with lengthwise α-direction of the top surface stress, and odd layers with widthwise α-direction of the top surface stress. Throughout the paper, these cases will be called <110>/αα, <110>/ββ, <110>/αβ, and <110>/βα, respectively. Illustrations of the surface configurations are given in Fig. 4.

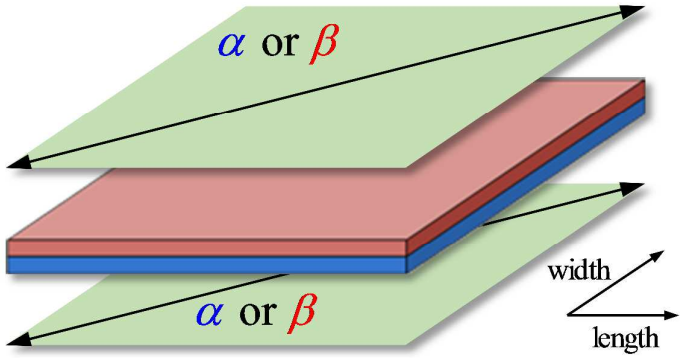

Figure 3. An Illustration showing possible surface configurations of Si/SiGe films in the case that a Si/SiGe strip is aligned in <100>. The directions of the top and bottom surfaces are either the same or orthogonal to each other. Therefore, two different surface configurations are possible.

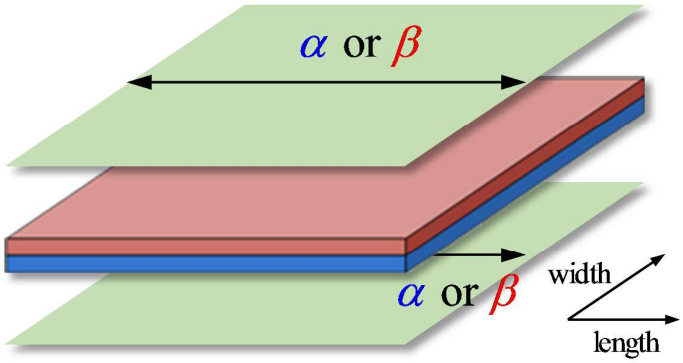

Figure 4. An Illustration showing possible surface configurations of Si/SiGe films in the case that a Si/SiGe strip is aligned in <110>. The lengthwise directions of the top and bottom surfaces can be in either the α or β direction. Therefore, four different surface configurations are possible.

c. Size effect on equilibrium configuration of nanosprings

To validate the accuracy of the FEAwSE, the results of FEAwSE and those of the MD simulation are compared. It is not practical to run the MD simulation with the experimentally reported geometry of nanosprings[5-14] (dozens of nanometers in thickness with a strip width of a few micrometers) due to the limitation of computing resources. Hence, very small sized models—in which the thicknesses are a few nanometers—are used for comparative purposes. Simulation details and the results are presented in supporting information SI1. Simulation results of Si/SiGe bilayer of both MD and FEAwSE are given in table 6, and the table shows the validity of FEAwSE.

Once the accuracy of the FEAwSE was approved, we performed simulations in a "realistic" length scale, which cannot be performed by MD owing to the limitation of the computing power. The size effect was investigated by varying the film thickness in various surface configurations.

Figs. 9 and 10 show the surface effect on pitch angles in the <100> and <110> directions, respectively, when the width-to-thickness ratio is 40. As expected, the pitch angle converges to the result with no surface effect as the thickness increases. The thickness effect is dramatic, and the effect is greater when odd numbers of atomic layers are used. Sometimes even the type of shape changes, e.g., from nanoband to nanospring.

In the <100> direction, two surface configurations, odd and even, are considered (Fig. 5). When the surface effect is neglected, the nanoring shape is obtained. However, when the surface effect is included and the thickness is small, the nanospring shape is obtained. It is noticeable that the surface effects can bring about different equilibrium configurations. This occurs because the principal direction of the surface effect is <110>. The pitch angle increases as the thickness decreases, and the odd case is more influenced by the surface effect.

In the <110> direction, the aforementioned four surface configurations are considered (Fig. 6). It is clearly observed that as the thickness increases, the resultant shape converges to the result of the no surface effect simulation. As the thickness decreases, the pitch angle begins to deviate from the results without a surface effect. The effect of surface on the geometry is more significant when odd numbered atomic layers are used. It is expected that the pitch angle can be tailored by controlling the surface configuration.

The deviation of the equilibrium configuration owing to the surface effect can be explained in this way. We took the <110>/βα surface configuration model, for example, and tried to observe the effects of surface and misfit strain separately. When the misfit strain is the only driving force (or when the surface effect is negligible), a helical shape is obtained, as shown in Fig. 6. To see the sheer effect of the surface, we calculated the equilibrium configuration of the Si monolayer (misfit strain is absent in the monolayer). We varied the thickness and fixed the width-to-thickness ratio as 40. The bending shape is obtained, and the normalized curvature radius (curvature radius/thickness) increases as the film thickness increases (Fig. 7). In summary, whereas misfit strain has the tendency to make the film roll in the <100> direction, the surface effect has the tendency to make the film roll in the <110> direction under the <110>/βα surface configuration model. The final equilibrium configuration can be regarded as the result of the competition between the misfit strain and the surface effect. Note the predominant tendency of rolling in the <100> direction as the thickness decreases in the <110>/βα model (Fig. 6). In addition, the surface effect is still not negligible when the thickness is around 100 nm (the normalized curvature radius of the Si monolayer is ~1000).

Table 6. Curvature radius (ρ) and pitch angle (ϑ) of resulting shapes of Si/SiGe bilayer thin film in four surface configuration models calculated from FEAwSE and MD.

	ρ (nm, FEA)	ρ (nm, MD)	θ (deg, FEA)	θ (deg, MD)
<100>/even	164.7	175.5	0.1	0.0
<100>/odd	125.3	133.2	29.9	29.3
<110>/αα	196.4	193.5	0.9	0.0
<110>/βα	102.7	112.5	0.3	0.0

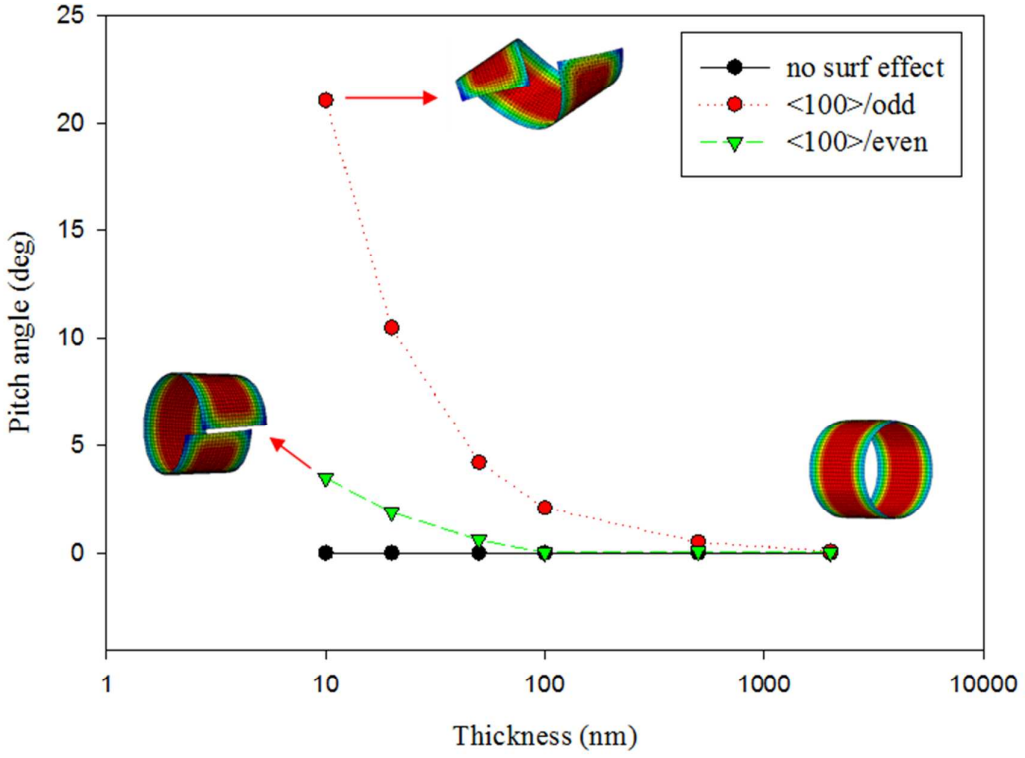

Figure 5. The effect of thickness calculated from FEAwSE when the width-to-thickness ratio is 40. The initial film is aligned in the <100> direction. The color of the inset figures indicates the maximum in-plane principal logarithmic strain

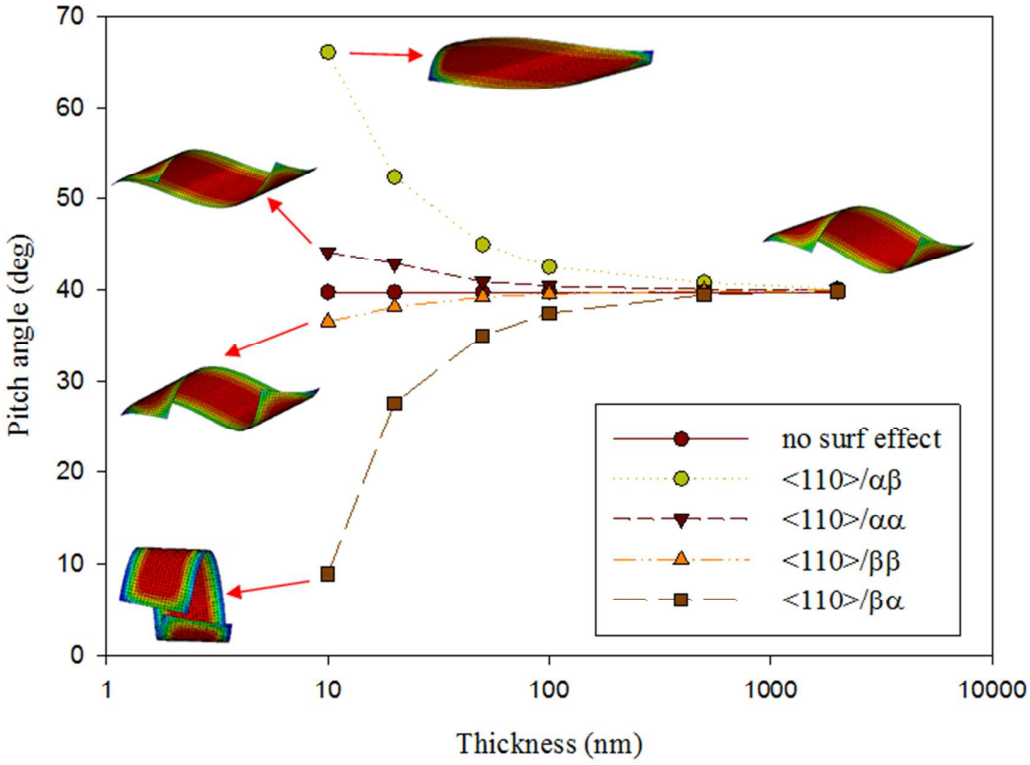

Figure 6. The effect of thickness calculated from FEAwSE when the width-to-thickness ratio is 40. The initial film is aligned in the <110> direction. The color of the inset figures indicates the maximum in-plane principal logarithmic strain.

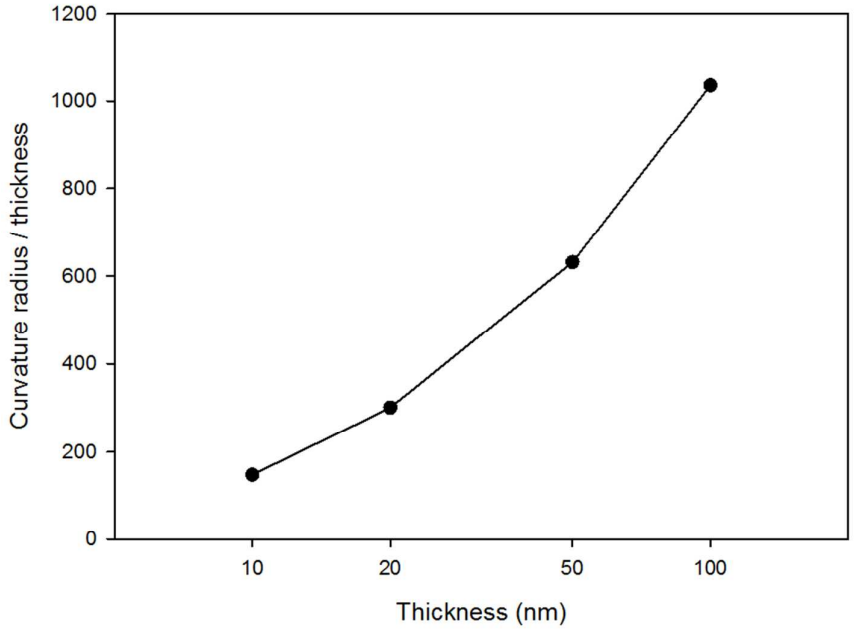

Figure 7. Normalized curvature radius of Si monolayer thin film with <110>/βα surface configuration. The width-to-thickness ratio was fixed at 40. Thickness is on a log scale.

3. Conclusions

The surface effect of Si/SiGe bilayer nanosprings was explored using continuum-level simulation schemes. The surface properties were determined by atomistic calculations, and the FEAwSE was performed using the calculated properties. The effect of the surface on the equilibrium configuration was remarkable when the thickness was less than ~100 nm. The effects of the surface configuration and size were critical factors in determining the equilibrium configuration. Even the equilibrium configuration type can be changed by both the thin film size and surface configuration. The number of atomic layers also should be considered since the surface configuration is dependent on this number. To fabricate nanosprings having nanoscale thickness, careful consideration of the surface effect is essential to predict the equilibrium configuration of nanosprings. Surface treatment is critical for deciding the equilibrium configuration because the surface effect is dominant in the nanoscale regime.

Acknowledgements

This work was supported by the National Research Foundation of Korea (NRF) grant funded by the Korea government. (MSIP) (No. 2012R1A3A2048841)

Notes and references

1. V. Dobrokhotov, L. Oakes, D. Sowell, A. Larin, J. Hall, A. Kengne, P. Bakharev, G. Corti, T. Cantrell, T. Prakash, J. Williams and D. N. McIlroy, *Sensor Actuat B-Chem*, 2012, **168**, 138-148.
2. Y. Sawa, K. Urayama, T. Takigawa, V. Gimenez-Pinto, B. L. Mbanga, F. F. Ye, J. V. Selinger and R. L. B. Selinger, *Phys Rev E*, 2013, **88**.
3. L. Zhang, J. J. Abbott, L. X. Dong, B. E. Kratochvil, D. Bell and B. J. Nelson, *Appl Phys Lett*, 2009, **94**.
4. K. F. Schilke, K. L. Wilson, T. Cantrell, G. Corti, D. N. McIlroy and C. Kelly, *Biotechnol Progr*, 2010, **26**, 1597-1605.
5. M. Zhang, Y. Nakayama and L. J. Pan, *Japanese Journal of Applied Physics Part 2-Letters*, 2000, **39**, L1242-L1244.
6. X. Y. Kong and Z. L. Wang, *Nano Lett*, 2003, **3**, 1625-1631.
7. H. F. Zhang, C. M. Wang, E. C. Buck and L. S. Wang, *Nano Lett*, 2003, **3**, 577-580.
8. P. V. Bakharev and D. N. McIlroy, *Nanotechnology*, 2014, **25**.
9. A. G. Mark, J. G. Gibbs, T. C. Lee and P. Fischer, *Nat Mater*, 2013, **12**, 802-807.
10. H. Liu, H. M. Cui, J. Y. Wang, L. Gao, F. Han, R. I. Boughton and M. H. Jiang, *J Phys Chem B*, 2004, **108**, 13254-13257.
11. M. H. Huang, C. Boone, M. Roberts, D. E. Savage, M. G. Lagally, N. Shaji, H. Qin, R. Blick, J. A. Nairn and F. Liu, *Advanced Materials*, 2005, **17**, 2860-2864.
12. D. J. Bell, L. X. Dong, B. J. Nelson, M. Golling, L. Zhang and D. Grutzmacher, *Nano Lett*, 2006, **6**, 725-729.
13. D. J. Bell, Y. Sun, L. Zhang, L. X. Dong, B. J. Nelson and D. Grutzmacher, *Sensors and Actuators a-Physical*, 2006, **130**, 54-61.
14. D. Grutzmacher, L. Zhang, L. Dong, D. Bell, B. Nelson, A. Prinz and E. Ruh, *Microelectronics Journal*, 2008, **39**, 478-481.
15. G. Hwang, H. Hashimoto, D. J. Bell, L. X. Dong, B. J. Nelson and S. Schon, *Nano Lett*, 2009, **9**, 554-561.
16. D. H. Wang and G. F. Wang, *Appl Phys Lett*, 2011, **98**.
17. S. Kim, W. Kim and M. Cho, *Japanese Journal of Applied Physics*, 2011, **50**.
18. Z. Chen, *Nanoscale*, 2014, **6**, 9443-9447.
19. A. Ramstad, G. Brocks and P. J. Kelly, *Phys Rev B*, 1995, **51**, 14504-14523.
20. C. Yang and H. C. Kang, *J Chem Phys*, 1999, **110**, 11029-11037.
21. G. F. Cerofolini, C. Galati, S. Reina, L. Renna, N. Spinella, D. Jones and V. Palermo, *Phys Rev B*, 2005, **72**.
22. C. Q. Chen, Y. Shi, Y. S. Zhang, J. Zhu and Y. J. Yan, *Physical Review Letters*, 2006, **96**.
23. R. Dingreville, J. M. Qu and M. Cherkaoui, *Journal of the Mechanics and Physics of Solids*,

2005, **53**, 1827-1854.

24. L. Lindsay and D. A. Broido, *Phys Rev B*, 2010, **82**.
25. D. Systemes, *Abaqus 6.10 Online Documentation*, 2010.
26. S. Plimpton, J. Comput. Phys., 1995, 117, 1-19.